

# The direct-line method for forward and inverse linear elasticity problems of composite materials in general domains with multiple singularities

Qinghua Wei<sup>1</sup>, Xiaopeng Zhu<sup>1,\*</sup>, and Zhongyi Huang<sup>2</sup>

<sup>1</sup> College of Science, Liaoning Technical University, Liaoning, China

<sup>2</sup> Department of Mathematical Sciences, Tsinghua University, Beijing 100084, China

---

**Abstract.** In this work, a combined strategy of domain decomposition and the direct-line method is implemented to solve the forward and inverse linear elasticity problems of composite materials in general domains with multiple singularities. Domain decomposition technology treats the general domain as the union of some star-shaped subdomains, which can be handled using the direct-line method. The direct-line method demonstrates rapid convergence of the semi-discrete eigenvalues towards the exact eigenvalues of the elliptic operator, thereby naturally capturing the singularities. We also establish optimal error estimates for the proposed method. Especially, our method can handle multiple singular point problems in general regions, which are difficult to deal with by most methods. On the other hand, the inverse elasticity problem is constructed as a energy functional minimization problem with total variational regularization, we use the aforementioned method as a forward solver to reconstruct the lamé coefficient of multiple singular points in general regions. Our method can simultaneously deduce heterogeneous  $\mu$  and  $\lambda$  between different materials. Through numerical experiments on three forward and inverse problems, we systematically verified the accuracy and reliability of this method to solve forward and inverse elastic problems in general domains with multiple singularities.

**AMS subject classifications:** 65N21, 65N40, 74A40, 74B05

**Key words:** composite materials, linear elasticity problems, inverse elasticity problems, the direct-line method.

---

## 1 Introduction

With the widespread application of composite materials in various fields, composite elasticity problems can be mathematically formulated as elliptic problems. When there is a sudden change in the geometric shape of interfaces or boundaries, singularities appear in the solutions of these elliptic problems. The stress singularity at these singular points poses a significant challenge to numerical research. The geometric complexity of composite materials, such as the presence of internal cracks and complex interfaces, often leads to elliptic problems with multiple singularities.

---

\*Corresponding author.

Emails: 1303698364@qq.com (X. Zhu), 3158563558@qq.com (Q. Wei), zhongyih@tsinghua.edu.cn (Z. Huang)

In recent decades, a wide range of methodologies have been proposed for solving problems involving single singular points. Include: Mesh refinement [1, 2], Infinite element method [3], Boundary element method [4, 5], Incorporation of singular functions in FEM [6, 7], Auxiliary mapping method [8], Mixed adaptive FEM [9], Galerkin discontinuous adaptive FEM [10], Modified extended FEM [11], Finite strip method [12], Stable generalized FEM [13], Extended isogeometric analysis [14], Extended finite element method(XFEM) [15], etc. The methods for solving multiple singular point problems have mainly been developed based on single singular point problems. Up to now, many methods cannot solve the problem of multiple singularities well.

Among all the methods, the direct-line method has received significant attention for solving elliptic problems with single singular point [16–18]. This method does not require prior knowledge of where the singularity is located [19], and circumvents the reduced convergence rate in discretization caused by singular points. So far, this method has been used on simple regions with a single singularity [20, 21]. Based on this method, we now develop a framework for handling multiple singularities in more general domain.

When dealing with elliptic problems that contain multiple singular points, the radial singularity persists in the local polar coordinate system centered at each singular point [22]. To address this challenge, we have proposed a domain decomposition method [24] suitable for our problem. Specifically, the general domain is decomposed into multiple interconnected subdomains [23, 25], with each subdomain containing exactly one singular point where the direct-line method can be applied individually. By enforcing continuity conditions across the interfaces between adjacent subdomains [26, 27], all subdomains are effectively coupled through a global coupling matrix  $G$ , thereby providing an effective solution strategy for problems with multiple singular points.

The numerical solution of inverse elasticity problems is another cornerstone of our research, with significant applications in non-destructive evaluation for detecting internal flaws such as cracks, voids, and delamination [28]. Leveraging the fact that full-field displacement measurements  $u$  are now accessible via established experimental techniques [29–31], we develop a numerical framework to simultaneously identify material interfaces and reconstruct the spatially varying Lamé coefficients. In contrast to existing approaches [32, 33], our method adopts a least-squares formulation [34] with piecewise constant approximations for the Lamé parameters. This inverse problem is framed as the minimization of a regularized energy functional that incorporates global variational constraints [35]. To efficiently solve this high-dimensional optimization problem, we employ the gradient-based Adam algorithm [36], which enhances computational efficiency through adaptive moment estimation. It is worth noting that a good forward problem solver is important for solving an inverse problem. Therefore, the combination of direct-line method and domain decomposition technique can be used as a good forward problem solver.

The outline of this paper is as follows: In Section 2, we introduce the direct-line coupling with domain decomposition techniques to numerically solve the linear elasticity problems with multiple singular points. Section 3 proposes a forward solver based on the method of Section 2 for solving inverse elasticity problems. In Section 4, the numerical experiments presented examine three distinct types of regions and validate the efficacy of the proposed method for solving both forward and inverse problems. Finally, We summarize and conclude the feasibility of combining direct-line

method with domain decomposition in Section 5.

## 2 The direct-line method for forward problems in general domains with multiple singularities

Consider a general domain  $\overline{\Omega} = \bigcup_{k=1}^K \overline{\Omega}_k \subset \mathbb{R}^2$  in a two-dimensional plane, where  $\Omega$  represents a domain composed of  $K$  different materials and  $\Omega_k$  represents the  $k$ -th material. Let  $O_{\tilde{k}}$ ,  $\tilde{k} = 1, \dots, \tilde{K}$  denote several singular points. The boundary  $\Gamma = \partial\Omega$  can be approximated as star-shaped relative to some singular points  $O_{\tilde{k}}$ . Considering the inherent complexity of arbitrary domains, in this work we hypothesize that all material interfaces coincide at singular points  $O_{\tilde{k}}$ , then each interface  $\partial\overline{\Omega}_k \cap \partial\overline{\Omega}_{k+1}$  is a simple polyline  $L_k$ . see Figure 1.

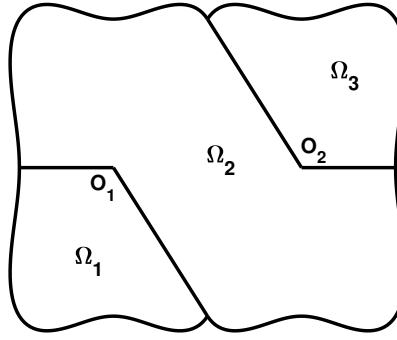


figure 1: Composite materials in a general domain with multiple singular points and material interfaces

The equilibrium state of composite materials under linear elasticity assumptions is governed by Navier's equations defined on a geometrically general domain  $\Omega$ , subject to Dirichlet boundary constraints:

$$\begin{aligned} -\nabla \cdot \sigma_k &= 0, \quad \text{in } \Omega_k, \\ u &= f, \quad \text{on } \Gamma, \\ u_k &= u_{k+1}, \quad \text{on } L_k, \\ \sigma_k \cdot n_k &= \sigma_{k+1} \cdot n_k \quad \text{on } L_k, \end{aligned} \tag{2.1}$$

with

$$\sigma_k = 2\mu_k \varepsilon(u_k) + \lambda_k \nabla \cdot u_k I, \quad \varepsilon(u_k) = \frac{1}{2} \left( \nabla u_k + (\nabla u_k)^T \right), \quad k = 1, \dots, K$$

where given a vector-valued function  $f$  on  $\Gamma$ ,  $\sigma|_{\Omega_k} = \sigma_k$  and  $\sigma$  is the stress tensor,  $u|_{\Omega_k} = u_k$  and  $u$  is the displacement,  $n_k$  is the unit normal vector of  $L_k$ . The Lamé coefficients  $\mu$  and  $\lambda$  are defined as piecewise-constant functions and taking distinct positive values  $(\mu_k, \lambda_k)$  in each subdomain  $\Omega_k$ .

The forward problem associated with (2.1) involves computing the displacement field  $u$  for known the Lamé coefficients  $(\mu, \lambda)$ . On the other hand, the inverse linear elasticity problem consists

in reconstructing the Lamé coefficients  $(\mu, \lambda)$  from the observed displacement data  $u$ . We assume that the entire domain  $\Omega$  can be separated into  $\tilde{K}$  subdomains  $\Omega^{(\tilde{k})}$  such that each subdomain contains only one singular point. Let the boundary  $\Gamma^{(\tilde{k})} = \partial\Omega^{(\tilde{k})}$  be star-shaped w.r.t. the singular point  $O_{\tilde{k}}$  and can be parameterized as a (piecewise)  $C^1$  function of the angular variable  $\phi^{(\tilde{k})}$ , this can be represented as  $\tilde{r}^{(\tilde{k})}(\phi^{(\tilde{k})})$ , obviously  $\tilde{r}^{(\tilde{k})}(0) = \tilde{r}^{(\tilde{k})}(2\pi)$  and  $\tilde{r}^{(\tilde{k})}(\phi^{(\tilde{k})}) \geq r_0 > 0$  for any discretization of angular variables  $0 \leq \phi^{(\tilde{k})} \leq 2\pi$ . Then we could introduce different curvilinear coordinates in each  $\Omega^{(\tilde{k})}$ , which constitutes the first step of the direct-line method.

$$(x^{(\tilde{k})}, y^{(\tilde{k})}) = e^{\rho^{(\tilde{k})}} \tilde{r}^{(\tilde{k})}(\phi^{(\tilde{k})}) (\cos(\phi^{(\tilde{k})}), \sin(\phi^{(\tilde{k})})), 0 \leq \phi^{(\tilde{k})} < 2\pi, -\infty < \rho^{(\tilde{k})} \leq 0. \quad (2.2)$$

## 2.1 Domain decomposition and coupling of two singular points

In this subsection, we present a coupled direct-line method with domain decomposition to numerically solve linear elastic problems of composite materials possessing two singular points.

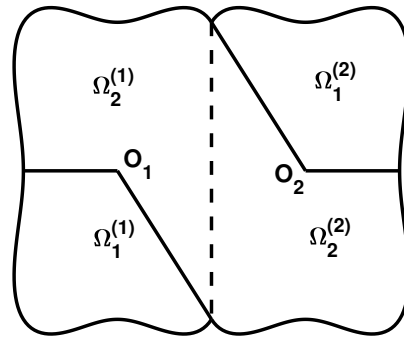


figure 2: Decomposition of domain  $\Omega$  into two subdomains, each containing one singular point

Assume that the entire domain  $\Omega$  can be separated into two subdomains  $\Omega^{(1)}$  and  $\Omega^{(2)}$  such that each subdomain contains only one singular point. The dashed line  $L_c = \partial\Omega^{(1)} \cap \partial\Omega^{(2)} = \partial\Omega_1^{(1)} \cap \partial\Omega_2^{(2)}$ ,  $\Omega^{(\tilde{k})} = \bigcup \Omega_i^{(\tilde{k})}, i = 1, 2$ . And the polyline  $L_{\tilde{k}} = \partial\Omega_1^{(\tilde{k})} \cap \partial\Omega_2^{(\tilde{k})}$ . This completes our domain decomposition (see Figure 2). Stress singularities will still occur at each singular point and the singularities exhibit radial distribution characteristics. Following the domain decomposition principle, problem (2.1) is

equivalent to the following coupled PDE systems:

$$\begin{aligned}
 -\nabla \cdot \sigma^{(1)} &= 0, \quad \text{in } \Omega^{(1)}, \\
 -\nabla \cdot \sigma^{(2)} &= 0, \quad \text{in } \Omega^{(2)}, \\
 u^{(1)} &= f, \quad \text{on } \partial\Omega^{(1)} \setminus \partial\Omega^{(2)}, \\
 u^{(2)} &= f, \quad \text{on } \partial\Omega^{(2)} \setminus \partial\Omega^{(1)}, \\
 u^{(1)} &= u^{(2)}, \quad \text{on } L_c, \\
 \sigma^{(1)} \cdot n_c &= \sigma^{(2)} \cdot n_c, \quad \text{on } L_c, \\
 u_1^{(\tilde{k})} &= u_2^{(\tilde{k})}, \quad \text{on } L_{\tilde{k}} \\
 \sigma_1^{(\tilde{k})} \cdot n_{\tilde{k}} &= \sigma_2^{(\tilde{k})} \cdot n_{\tilde{k}} \quad \text{on } L_{\tilde{k}}
 \end{aligned} \tag{2.3}$$

We now proceed with the numerical solution of problem (2.3). It is crucial to note that the overlapping boundary portions between domains  $\Omega^{(1)}$  and  $\Omega^{(2)}$  serve as the key coupling mechanism to connect the subdomains. In subdomain  $\Omega^{(1)}$ , we discretize the interval  $[0, 2\pi]$  as  $0 = \phi_1^{(1)} < \phi_2^{(1)} < \dots < \phi_{M+1}^{(1)} = 2\pi$ , denote  $\Phi = \{1, \dots, M\}$  and let  $I^{(1)} = \{j_1, \dots, j_m\} \subset \Phi^{(1)}$  be those such that  $\forall j_i \in I^{(1)}, (0, \phi_{j_i}^{(1)}) \in \partial\Omega^{(1)} \cap \partial\Omega^{(2)}$  in the curvilinear coordinate system (2.2) of  $\Omega^{(1)}$ . Similarly, let  $I^{(2)} = \{k_1, \dots, k_m\} \subset \Phi^{(2)}$  be those such that  $\forall k_i \in I^{(2)}, (0, \phi_{k_i}^{(2)}) \in \partial\Omega^{(1)} \cap \partial\Omega^{(2)}$  in the curvilinear coordinate system (2.2) of  $\Omega^{(2)}$ . The numerical solution in the subdomains  $\Omega^{(\tilde{k})}$  can be expressed as

$$u_h^{(\tilde{k})}(\rho, \phi) = N^{(\tilde{k})}(\phi)^T S^{(\tilde{k})}(\rho) \alpha^{(\tilde{k})}, \tilde{k} = 1, 2. \tag{2.4}$$

The construction of  $N^{(\tilde{k})}, S^{(\tilde{k})}, \alpha^{(\tilde{k})}, \tilde{k} = 1, 2$  follows a consistent formulation pattern in reference [20]. We similarly obtain  $N^{(\tilde{k})}$  and  $S^{(\tilde{k})}$ . The coefficient vector  $\alpha^{(\tilde{k})} = [\alpha_1^{(\tilde{k})}, \alpha_2^{(\tilde{k})}, \dots, \alpha_{2M}^{(\tilde{k})}]^T$  is determined by enforcing the boundary conditions and the interface conditions that couple the subdomains. A coupling matrix of dimension  $4M \times 4M$  is constructed to enforce these constraints.

$$G = \begin{bmatrix} V_{\Phi \setminus I^{(1)}}^{(1)} & 0 \\ 0 & V_{\Phi \setminus I^{(2)}}^{(2)} \\ V_{I^{(1)}}^{(1)} & -V_{I^{(2)}}^{(2)} \\ H_{I^{(1)}}^{(1)} & H_{I^{(2)}}^{(2)} \end{bmatrix} \tag{2.5}$$

Where  $\Phi \setminus I^{(1)} = \{n_1, \dots, n_{M-m}\}$  represents the remaining portion of the boundary of  $\Omega^{(1)}$  excluding  $I^{(1)}$ . Similarly, let  $\Phi \setminus I^{(2)} = \{l_1, \dots, l_{M-m}\}$ . Let  $V_{I^{(1)}}^{(1)}$  be rows of  $S^{(1)}$  whose indices are  $\{j_1, \dots, j_m\}$ ,  $V_{I^{(2)}}^{(2)}$  be rows of  $S^{(2)}$  whose indices are  $\{k_1, \dots, k_m\}$ ,  $V_{\Phi \setminus I^{(1)}}^{(1)}$  be rows of  $S^{(1)}$  whose indices are  $\{n_1, \dots, n_{M-m}\}$ ,  $V_{\Phi \setminus I^{(2)}}^{(2)}$  be rows of  $S^{(2)}$  whose indices are  $\{l_1, \dots, l_{M-m}\}$ . Let  $H_{I^{(1)}}^{(1)}$  be rows of  $H^{(1)}$  whose indices are  $\{j_1, \dots, j_m\}$ ,  $H_{I^{(2)}}^{(2)}$  be rows of  $H^{(2)}$  whose indices are  $\{k_1, \dots, k_m\}$ , where

$$H^{(\tilde{k})} = \sum_{\tilde{k}=1}^{\tilde{K}} \int_{\theta_{\tilde{k}}}^{\theta_{\tilde{k}+1}} \left( N(\phi) \Psi_1 N'(\phi)^T + N(\phi) \Psi_2 N(\phi)^T S'(0) S(0)^{-1} \right)^{(\tilde{k})} d\phi,$$

from reference [20]. Set the  $4M \times 1$  vector

$$F = [F_{\Phi \setminus I^{(1)}}^{(1)T}, F_{\Phi \setminus I^{(2)}}^{(2)T}, 0, \dots, 0]^T, \tag{2.6}$$

where  $F_{\Phi \setminus I^{(1)}}^{(1)}$  be rows of  $F^{(1)}$  whose indices are  $\{n_1, \dots, n_{M-m}\}$ ,  $F_{\Phi \setminus I^{(2)}}^{(2)}$  be rows of  $F^{(2)}$  whose indices are  $\{l_1, \dots, l_{M-m}\}$ ,  $F^{(\tilde{k})}$  is the Dirichlet boundary condition in  $\Omega^{(\tilde{k})}$ . Then by the boundary conditions and interface conditions,  $\alpha^{(1)}$  and  $\alpha^{(2)}$  satisfy

$$G[\alpha^{(1)T}, \alpha^{(2)T}]^T = F \quad (2.7)$$

After solving (2.7), we would obtain the numerical solution  $u_h^{(1)}(\rho, \phi)$  and  $u_h^{(2)}(\rho, \phi)$  in subdomain  $\Omega^{(1)}$  and  $\Omega^{(2)}$ .

## 2.2 Domain decomposition and coupling of four singular points

In this subsection, we extend the methodology for elliptic problems with two singular points to the more challenging case of four singular points. We consider the following problem (2.1). We assume that the entire domain  $\Omega = \bigcup \Omega_k, k=1, \dots, 5$  (see Figure 3a) can be partitioned into four subdomains  $\Omega = \bigcup \Omega^{(\tilde{k})}, \tilde{k}=1, \dots, 4$ , and  $\Omega^{(\tilde{k})} = \bigcup \Omega_i^{(\tilde{k})}, i=1, 2$  (see Figure 3b).

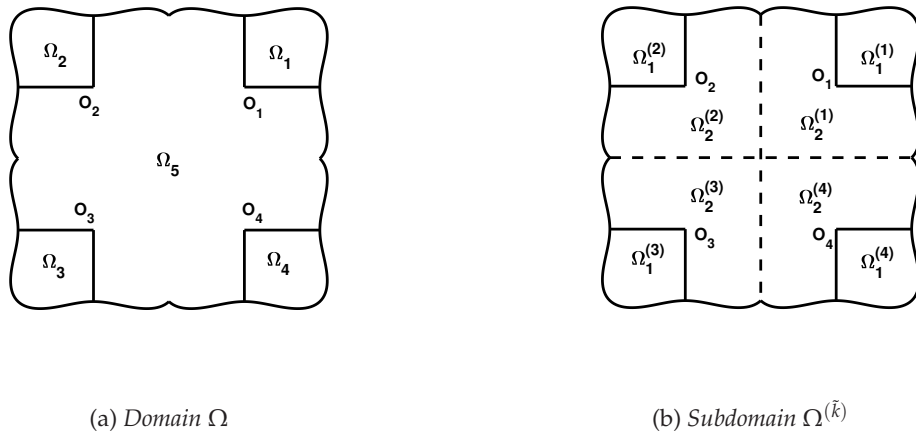


figure 3: (a) Original domain with four singular points; (b) Partition into four subdomains

Following the domain decomposition principle, problem (2.1) is equivalent to four coupled sub-

problems. Under these conditions, (2.1) becomes equivalent to the following coupled PDE system

$$\begin{aligned}
-\nabla \cdot \sigma^{(\tilde{k})} &= 0, \quad \text{in } \Omega^{(\tilde{k})}, \\
u^{(\tilde{k})} &= f, \quad \text{on } \partial\Omega^{(\tilde{k})} \cap \partial\Omega, \\
u^{(1)} &= u^{(2)}, \quad \text{on } L_{c1}, \\
u^{(2)} &= u^{(3)}, \quad \text{on } L_{c2}, \\
u^{(3)} &= u^{(4)}, \quad \text{on } L_{c3}, \\
u^{(4)} &= u^{(1)}, \quad \text{on } L_{c4}, \\
\sigma^{(1)} \cdot n_{c1} &= \sigma^{(2)} \cdot n_{c1}, \quad \text{on } L_{c1}, \\
\sigma^{(2)} \cdot n_{c2} &= \sigma^{(3)} \cdot n_{c2}, \quad \text{on } L_{c2}, \\
\sigma^{(3)} \cdot n_{c3} &= \sigma^{(4)} \cdot n_{c3}, \quad \text{on } L_{c3}, \\
\sigma^{(4)} \cdot n_{c4} &= \sigma^{(1)} \cdot n_{c4}, \quad \text{on } L_{c4}, \\
u_1^{(\tilde{k})} &= u_2^{(\tilde{k})}, \quad \text{on } L_{\tilde{k}} \\
\sigma_1^{(\tilde{k})} \cdot n_{\tilde{k}} &= \sigma_2^{(\tilde{k})} \cdot n_{\tilde{k}} \quad \text{on } L_{\tilde{k}}
\end{aligned} \tag{2.8}$$

where the dashed line  $L_c = \bigcup L_{ci}, i = 1, \dots, 4$ , represent the interfaces between subdomains,  $L_{c1} = \partial\Omega^{(1)} \cap \partial\Omega^{(2)}$ ,  $L_{c2} = \partial\Omega^{(2)} \cap \partial\Omega^{(3)}$ ,  $L_{c3} = \partial\Omega^{(3)} \cap \partial\Omega^{(4)}$ ,  $L_{c4} = \partial\Omega^{(4)} \cap \partial\Omega^{(1)}$ , and the polyline  $L_{\tilde{k}} = \partial\Omega_1^{(\tilde{k})} \cap \partial\Omega_2^{(\tilde{k})}$ .

We now proceed with the numerical solution of problem (2.8). In subdomain  $\Omega^{(1)}$ , we discretize the interval  $[0, 2\pi]$  as  $0 = \phi_1^{(1)} < \phi_2^{(1)} < \dots < \phi_{M+1}^{(1)} = 2\pi$ , denote  $\Phi = \{1, \dots, M\}$  and let  $I^{(1,2)} = \{j_1, \dots, j_m\} \subset \Phi$  be those such that  $\forall j_i \in I^{(1,2)}, (0, \phi_{j_i}^{(1)}) \in \partial\Omega^{(1)} \cap \partial\Omega^{(2)}$  in the curvilinear coordinate system (2.2) of  $\Omega^{(1)}$ , and let  $I^{(1,4)} = \{j'_1, \dots, j'_m\} \subset \Phi$  be those such that  $\forall j'_i \in I^{(1,4)}, (0, \phi_{j'_i}^{(1)}) \in \partial\Omega^{(1)} \cap \partial\Omega^{(4)}$  in the curvilinear coordinate system (2.2) of  $\Omega^{(1)}$ . We will not go into details about the other subdomains. We now proceed with the numerical solution of equation (2.8). The solutions can also be expressed as

$$u_h^{(\tilde{k})}(\rho, \phi) = N^{(\tilde{k})}(\phi)^T S^{(\tilde{k})}(\rho) \alpha^{(\tilde{k})}, \tilde{k} = 1, \dots, 4. \tag{2.9}$$

The construction of  $N^{(\tilde{k})}, S^{(\tilde{k})}, \alpha^{(\tilde{k})}, \tilde{k} = 1, \dots, 4$  follow a consistent formulation pattern. We similarly obtain  $N^{(\tilde{k})}$  and  $S^{(\tilde{k})}$ . To obtain  $\alpha^{(\tilde{k})} = [\alpha_1^{(\tilde{k})}, \alpha_2^{(\tilde{k})}, \dots, \alpha_{2M}^{(\tilde{k})}]$ , we incorporate both boundary conditions and interface conditions that govern the subdomain interactions. A coupling matrix of dimension  $8M \times 8M$  is constructed to enforce these constraints.

$$G = \begin{bmatrix} V_{\Phi \setminus I_1}^{(1)} & 0 & 0 & 0 \\ 0 & V_{\Phi \setminus I_2}^{(2)} & 0 & 0 \\ 0 & 0 & V_{\Phi \setminus I_3}^{(3)} & 0 \\ 0 & 0 & 0 & V_{\Phi \setminus I_4}^{(4)} \\ V_{I^{(1,2)}}^{(1)} & -V_{I^{(2,1)}}^{(2)} & 0 & 0 \\ 0 & V_{I^{(2,3)}}^{(2)} & -V_{I^{(3,2)}}^{(3)} & 0 \\ 0 & 0 & V_{I^{(3,4)}}^{(3)} & -V_{I^{(4,3)}}^{(4)} \\ -V_{I^{(1,4)}}^{(1)} & 0 & 0 & V_{I^{(4,1)}}^{(4)} \\ H_{I^{(1,2)}}^{(1)} & H_{I^{(2,1)}}^{(2)} & 0 & 0 \\ 0 & H_{I^{(2,3)}}^{(2)} & H_{I^{(3,2)}}^{(3)} & 0 \\ 0 & 0 & H_{I^{(3,4)}}^{(3)} & H_{I^{(4,3)}}^{(4)} \\ H_{I^{(1,4)}}^{(1)} & 0 & 0 & H_{I^{(4,1)}}^{(4)} \end{bmatrix} \quad (2.10)$$

where  $I_1 = I^{(1,2)} \cup I^{(1,4)}$ ,  $I_2 = I^{(2,3)} \cup I^{(2,1)}$ ,  $I_3 = I^{(3,4)} \cup I^{(3,2)}$ ,  $I_4 = I^{(4,1)} \cup I^{(4,3)}$ .  $\Phi \setminus I_1 = \{n_1, \dots, n_{M-2m}\}$  represents the remaining portion of the boundary of  $\Omega^{(1)}$  excluding  $I_1$ . Here, matrix  $G$  is not elaborated upon further, similar to Subsection 2.1.

and the  $8M$ -by-1 vector

$$F = [F_{\Phi \setminus I_1}^{(1)T}, F_{\Phi \setminus I_2}^{(2)T}, F_{\Phi \setminus I_3}^{(3)T}, F_{\Phi \setminus I_4}^{(4)T}, 0, \dots, 0]^T \quad (2.11)$$

Then, by the boundary conditions and interface conditions,  $\alpha^{(\tilde{k})}$  satisfies

$$G[\alpha^{(1)T}, \alpha^{(2)T}, \alpha^{(3)T}, \alpha^{(4)T}]^T = F \quad (2.12)$$

After solving (2.12), we would obtain the numerical solution  $u_h^{(\tilde{k})}(\rho, \phi)$  and in subdomain  $\Omega^{(\tilde{k})}$ . In subsections 2.1 and 2.2, the specific form of  $G$  varies with the geometry of the domain.

### 2.3 Error estimation

**Theorem 2.1.** Assume the use of linear elements, there exists a constant  $C > 0$  independent of the mesh size  $h$  such that the following error estimate holds:

$$\|u - u_h\|_*^2 \leq Ch^2 \sum_{j=1}^2 \iint_{\Omega} \left( |\nabla u_j|^2 + \sum_{|\beta|=2} (x^2 + y^2) |D^\beta u_j|^2 \right) dx dy, \quad (2.13)$$

where  $|\beta| = \beta_1 + \beta_2$ ,  $\beta = (\beta_1, \beta_2)^T \in N^2$ ,  $D^\beta u_j = \frac{\partial^{|\beta|} u_j}{\partial x^{\beta_1} \partial y^{\beta_2}}$  and for any  $w, v \in H^1(\Omega) \times H^1(\Omega)$ ,

$$\begin{aligned} \|w\|_* &= E(w, w)^{1/2} + |\psi_1(w)| + |\psi_2(w)| + |\psi_3(w)|, \\ \psi_1(w) &= \int_{\Gamma} w_1 ds, \quad \psi_2(w) = \int_{\Gamma} w_2 ds, \quad \psi_3(w) = \int_{\Gamma} (w_1 y - w_2 x) ds, \end{aligned}$$

$$\begin{aligned} E(w, v) &= \sum_{k=1}^K \iint_{\Omega_k} \left( \lambda_k (\nabla \cdot w^k) \cdot (\nabla \cdot v^k) + 2\mu_k \left( \partial_x w_1^k \partial_x v_1^k + \partial_y w_2^k \partial_y v_2^k \right) \right. \\ &\quad \left. + \mu_k \left( \partial_y w_1^k + \partial_x w_2^k \right) \left( \partial_y v_1^k + \partial_x v_2^k \right) \right) dx dy. \end{aligned}$$

Recall that  $u$  belongs to  $H^1(\Omega)$ , but the solution of  $u$  is not in the  $H^2(\Omega)$  space, so  $|\beta|=2$  is integrable, and when  $|\beta|=2$ ,  $|D^\beta u|^2$  is not integrable. However, considering that  $u$  has only singularities of the form  $\mathcal{O}(r^{b_j})$  in the  $r$  direction near singular points, where  $0 < \text{Re}(b_j) < 1$  and  $\phi$  is smooth, it follows that  $r^2|D^\beta u|^2$  is integrable for  $|\beta|=2$ . In Theorem 2.1, the integral (2.13) is finite. Therefore, from Theorem 2.1, it can be concluded that even if  $u \notin H^2(\Omega)$ , we can still use linear elements for semi-discretization to obtain optimal first-order convergence in the energy norm  $\|\cdot\|_*$ . Furthermore, we assume that for each region there are normal numbers  $(\lambda, \mu)$ , we can conclude  $\|\sigma - \sigma^h\|_{L^2} \leq C\|u - u^h\|_*$ , where  $h$  is independent of the constant  $C$ , and  $\sigma^h$  denotes the computed stress tensor associated with the discrete displacement field  $u^h$ . At the same time, we can use linear elements to achieve first-order convergence in  $L^2$  norm for singular stress  $\sigma$ .

### 3 Inverse Elasticity Problems

The inverse problem aims to reconstruct the Lamé coefficients from displacement field measurement data. The study considers composite elastic materials within a general domain, where material interfaces are represented as polygonal lines connecting singular points to boundary points. The main goal is to restore the values of the Lamé parameters and the geometric shapes of these interfaces simultaneously on all subdomains.

#### 3.1 A regularized minimization problem

We let  $u[\ell]$  be a solution to (2.1), here define the Lamé coefficients  $\ell = (\mu, \lambda)$ . For problems involving abrupt material property transitions, as manifested through discontinuous Lamé coefficients, We are given certain constants  $C_1, C_2 > 0$ , and for any  $v \in L^1(\Omega)$ , which is defined as

$$\ell \in \Lambda := \{ \ell = (\mu, \lambda) \in L^\infty(\Omega) \times L^\infty(\Omega) \mid C_1 \leq \mu, \lambda \leq C_2, \text{TV}(\mu) < \infty, \text{TV}(\lambda) < \infty \}, \quad (3.1)$$

$$\text{TV}(v) = \sup \left\{ \iint_{\Omega} (v(\nabla \cdot w)) dx dy \mid w \in (C_0^1(\Omega))^2, |w(x)| \leq 1, \forall x \in \Omega \right\}, \quad (3.2)$$

where  $\text{TV}(v)$  is the total variation of  $v$  [35] and  $|\cdot|$  denotes the Euclidean norm of a vector. In the inverse elasticity problem with full-field data, we consider a noisy measurement  $z(x, y)$  of the displacement field  $u[\ell^*](x, y)$ , where  $(x, y) \in \Omega$  and  $\ell^* = (\mu^*, \lambda^*) \in \Lambda$ . The objective is to reconstruct the unknown parameters  $\ell^*$  from the measured data  $z$ . Construct an optimization problem to solve the reconstruction of  $\ell^*$ , where the goal is to minimize a regularized energy functional [37]. Since the coefficients of each subdomain are not identical, that is, they have jump discontinuities in the Lamé coefficients. Thus, by using the total variation method, we can effectively recover the Lamé coefficients [35]. We get an optimization problem

$$\min_{\ell \in \Lambda} J(\ell) := \frac{1}{2} \iint_{\Omega} (\lambda |\nabla \cdot (u[\ell] - z)|^2 + 2\mu |\varepsilon(u[\ell] - z)|^2) dx dy + \eta (\text{TV}(\mu) + \text{TV}(\lambda)), \quad (3.3)$$

where  $\eta$  is the regularization parameter and greater than 0, and let

$$J_0(\ell) = \frac{1}{2} \iint_{\Omega} (\lambda |\nabla \cdot (u[\ell] - z)|^2 + 2\mu |\varepsilon(u[\ell] - z)|^2) dx dy.$$

A theorem in the literature [34] gives the existence of solutions for (3.3). Here is a brief explanation.

**Theorem 3.1.** The minimization problem (3.3) exists at least one solution  $\ell^0 \in \Lambda$ .

### 3.2 Numerical program

Continuing our analysis within the curvilinear coordinate established in (2.2). In the subdomain  $\Omega^{(\tilde{k})}$ , for a fixed  $\rho^{(\tilde{k})}$ , they are piecewise constant functions along the  $\phi^{(\tilde{k})}$ -direction, and for a fixed  $\phi^{(\tilde{k})}$ , both  $\mu^*$  and  $\lambda^*$  remain constant along the  $\rho^{(\tilde{k})}$ -direction. Hence we let  $0 = \varphi_0^{(\tilde{k})} < \varphi_1^{(\tilde{k})} < \dots < \varphi_{m'}^{(\tilde{k})} = 2\pi$  and define the discrete parameter space

$$\Lambda_{h'} = \left\{ \ell_{h'}(\rho, \phi) = (\mu_{h'}, \lambda_{h'}) \in \Lambda \middle| \begin{array}{l} \mu_{h'}, \lambda_{h'} \text{ are constants almost everywhere} \\ \text{on } (-\infty, 0] \times [\varphi_{j-1}^{(\tilde{k})}, \varphi_j^{(\tilde{k})}) \text{ for } j=1, \dots, m'. \end{array} \right\}, \quad (3.4)$$

where  $h' = \max_{1 \leq \tilde{k} < \tilde{K}} \max_{1 \leq j < m} |\varphi_j^{(\tilde{k})} - \varphi_{j-1}^{(\tilde{k})}|$ . We discretize (3.3) by the following discrete minimization problem:

$$\begin{aligned} \min_{\ell_{h'} \in \Lambda_{h'}} J(\ell_{h'}) = & \frac{1}{2} \sum_{\tilde{k}=1}^{\tilde{K}} \sum_{j=1}^{m'} \int_{-\infty}^0 \int_{\varphi_{j-1}^{(\tilde{k})}}^{\varphi_j^{(\tilde{k})}} (2\mu_{h'} |\varepsilon(u[\ell_{h'}] - z)|^2 + \lambda_{h'} |\nabla \cdot (u[\ell_{h'}] - z)|^2) \\ & e^{2\rho^{(\tilde{k})}} \tilde{r}^{(\tilde{k})}(\phi)^2 d\phi d\rho^{(\tilde{k})} + \eta (\text{TV}(\mu_{h'}) + \text{TV}(\lambda_{h'})). \end{aligned} \quad (3.5)$$

To the solution of problem (3.3), the minimizer  $\ell_{h'}^0 \in \Lambda_{h'}$ , obtained by solving problem (3.5), serves as a numerical approximation. The following theorem concerns the existence of solutions to equation (3.5), and its proof utilizes Theorem 3.2 as well as a fact that under the  $L^1$  metric,  $\Lambda_{h'}$  forms a closed subset of  $\Lambda$ .

**Theorem 3.2.** The minimizing problem (3.5) exists at least one solution  $\ell_{h'}^0 \in \Lambda_{h'}$ .

In each subdomain  $\Omega^{(\tilde{k})}$ , let us postulate that

$$\mu_{h'}(\rho, \phi) = \mathbb{1}_{(-\infty, 0]}(\rho) \sum_{j=1}^{m'} \mu_j \mathbb{1}_{[\varphi_{j-1}, \varphi_j]}(\phi), \quad \lambda_{h'}(\rho, \phi) = \mathbb{1}_{(-\infty, 0]}(\rho) \sum_{j=1}^{m'} \lambda_j \mathbb{1}_{[\varphi_{j-1}, \varphi_j]}(\phi). \quad (3.6)$$

Then we have

$$\text{TV}(\mu_{h'}) = \sum_{j=1}^{m'} \tilde{r}(\varphi_j) |\mu_{j+1} - \mu_j|, \quad \text{TV}(\lambda_{h'}) = \sum_{j=1}^{m'} \tilde{r}(\varphi_j) |\lambda_{j+1} - \lambda_j|,$$

where  $\mu_{m'+1} = \mu_1, \lambda_{m'+1} = \lambda_1$ . Calculating the gradient of  $J$  is crucial in the Adam algorithm, so we will calculate the gradients of  $\text{TV}(\mu_{h'})$  and  $\text{TV}(\lambda_{h'})$ . At the origin, the absolute value  $|\cdot|$  is non-differentiability, so we will approximate  $\text{TV}(\mu_{h'})$  and  $\text{TV}(\lambda_{h'})$ :

$$\text{TV}_v(\mu_{h'}) = \sum_{j=1}^{m'} \tilde{r}(\varphi_j) \sqrt{|\mu_{j+1} - \mu_j|^2 + v^2}, \quad \text{TV}_v(\lambda_{h'}) = \sum_{j=1}^{m'} \tilde{r}(\varphi_j) \sqrt{|\lambda_{j+1} - \lambda_j|^2 + v^2},$$

where  $v \in (0, 1]$  is a small regularization parameter. Rather than minimizing  $J$  directly, The optimal solution  $\ell_{h'}^* \in \Lambda_{h'}$  is obtained by minimizing the regularized energy functional over all candidate

parameters  $\ell'_h \in \Lambda_{h'}$ :

$$J_V(\ell'_h) := \frac{1}{2} \sum_{\tilde{k}=1}^{\tilde{K}} \sum_{j=1}^{m'} \int_{-\infty}^0 \int_{\varphi_{j-1}^{(\tilde{k})}}^{\varphi_j^{(\tilde{k})}} (2\mu_{h'} |\varepsilon(u[\ell_{h'}] - z)|^2 + \lambda_{h'} |\nabla \cdot (u[\ell_{h'}] - z)|^2) e^{2\rho^{(\tilde{k})}} \tilde{r}^{(\tilde{k})} (\phi)^2 d\phi^{(\tilde{k})} d\rho^{(\tilde{k})} + \eta(\text{TV}(\mu_{h'}) + \text{TV}(\lambda_{h'})). \quad (3.7)$$

Next, setting  $j = 1, \dots, m'$ , we calculate the gradients of  $\text{TV}(\mu_{h'})$  and  $\text{TV}(\lambda_{h'})$ , and  $\mu_0 = \mu_{m'}, \lambda_0 = \lambda_{m'}$  and  $\mu_{m'+1} = \mu_1, \lambda_{m'+1} = \lambda_1$ .

$$\frac{\partial \text{TV}_V(\mu_{h'})}{\partial \mu_j} = \tilde{r}(\varphi_{j-1}) \frac{\mu_j - \mu_{j-1}}{\sqrt{|\mu_j - \mu_{j-1}|^2 + \nu^2}} + \tilde{r}(\varphi_j) \frac{\mu_j - \mu_{j+1}}{\sqrt{|\mu_j - \mu_{j+1}|^2 + \nu^2}},$$

$$\frac{\partial \text{TV}_V(\lambda_{h'})}{\partial \lambda_j} = \tilde{r}(\varphi_{j-1}) \frac{\lambda_j - \lambda_{j-1}}{\sqrt{|\lambda_j - \lambda_{j-1}|^2 + \nu^2}} + \tilde{r}(\varphi_j) \frac{\lambda_j - \lambda_{j+1}}{\sqrt{|\lambda_j - \lambda_{j+1}|^2 + \nu^2}},$$

The gradients with respect to the nodal values  $\mu_j$  and  $\lambda_j$  are computed by applying the chain rule:

$$\begin{aligned} \frac{\partial J_0}{\partial \mu_j} &= \int_{-\infty}^0 \int_0^{2\pi} \frac{\partial J_0}{\partial \mu_{h'}} \frac{\partial \mu_{h'}}{\partial \mu_j} e^{2\rho^{(\tilde{k})}} \tilde{r}^{(\tilde{k})} (\phi)^2 d\phi^{(\tilde{k})} d\rho^{(\tilde{k})} = \int_{-\infty}^0 \int_{\varphi_{j-1}}^{\varphi_j} \frac{\partial J_0}{\partial \mu_{h'}} e^{2\rho^{(\tilde{k})}} \tilde{r}^{(\tilde{k})} (\phi)^2 d\phi^{(\tilde{k})} d\rho^{(\tilde{k})}, \\ \frac{\partial J_0}{\partial \lambda_j} &= \int_{-\infty}^0 \int_0^{2\pi} \frac{\partial J_0}{\partial \lambda_{h'}} \frac{\partial \lambda_{h'}}{\partial \lambda_j} e^{2\rho^{(\tilde{k})}} \tilde{r}^{(\tilde{k})} (\phi)^2 d\phi^{(\tilde{k})} d\rho^{(\tilde{k})} = \int_{-\infty}^0 \int_{\varphi_{j-1}}^{\varphi_j} \frac{\partial J_0}{\partial \lambda_{h'}} e^{2\rho^{(\tilde{k})}} \tilde{r}^{(\tilde{k})} (\phi)^2 d\phi^{(\tilde{k})} d\rho^{(\tilde{k})}, \end{aligned}$$

and we know from [34] that

$$\frac{\partial J_0}{\partial \mu_{h'}} = -\varepsilon(u[\ell_{h'}] + z) \cdot \varepsilon(u[\ell_{h'}] - z), \quad \frac{\partial J_0}{\partial \lambda_{h'}} = -\frac{1}{2} (\nabla \cdot (u[\ell_{h'}] + z)) \cdot (\nabla \cdot (u[\ell_{h'}] - z)).$$

Hence for  $j = 1, \dots, m'$

$$\frac{\partial J_V}{\partial \mu_j} = \frac{\partial J_0}{\partial \mu_j} + \eta \frac{\partial \text{TV}_V(\mu_{h'})}{\partial \mu_j}, \quad \frac{\partial J_V}{\partial \lambda_j} = \frac{\partial J_0}{\partial \lambda_j} + \eta \frac{\partial \text{TV}_V(\lambda_{h'})}{\partial \lambda_j}. \quad (3.8)$$

After a series of discussions, in order to obtain the gradient and value of  $J_V$ , it is necessary to evaluate  $u[\ell_h]$ . We pay special attention to two issues: First, since  $\ell_h \in \Lambda_h$ , an interface problem must be considered in the formulation of the forward problem. Therefore, the solution  $u[\ell_h]$  exhibits stress characteristics at the intersection points of the interface. Second, the general domains are very complicated with multiple singularities. The direct-line method serves as the forward solver to address both challenges. Denoting  $\mathcal{G}^{(\tilde{k})} = \left( \frac{\partial J_V}{\partial \mu_1^{(\tilde{k})}}, \dots, \frac{\partial J_V}{\partial \mu_{m'}^{(\tilde{k})}}, \frac{\partial J_V}{\partial \lambda_1^{(\tilde{k})}}, \dots, \frac{\partial J_V}{\partial \lambda_{m'}^{(\tilde{k})}} \right)^T$ ,  $\mathcal{L}^{(\tilde{k})} = (\mu_1^{(\tilde{k})}, \dots, \mu_{m'}^{(\tilde{k})}, \lambda_1^{(\tilde{k})}, \dots, \lambda_{m'}^{(\tilde{k})})^T$ , and  $\mathcal{L}_t^{(\tilde{k})}$  denote the value of  $\mathcal{L}^{(\tilde{k})}$  at the  $t$ -th iteration, and  $\mathcal{G}_t^{(\tilde{k})}$  denote the value of  $\mathcal{G}^{(\tilde{k})}$  at  $\ell_{h'}^t$ . And  $\ell_{h'}^t = (\mu_{h'}^t, \lambda_{h'}^t)$  represent the discrete Lamé coefficients defined in (3.6) corresponding to  $\mathcal{L}_t^{(\tilde{k})}$ . Algorithm 3.1 outlines the integrated computational framework, which incorporates both the Adam optimizer and the direct-line method approach to address the inverse elasticity problem.

**Algorithm 3.1** Implementation of the inverse elasticity problem

---

- 1: **Input:** the measurement data  $z$ , the starting value  $\mathcal{L}_0^{(\tilde{k})}$ , the parameters of the regularized functional  $J_\nu$  (namely  $\nu$  and  $\eta$ ), and the algorithmic parameters: exponential decay rates  $\hat{\beta}_1, \hat{\beta}_2$ , the tolerance threshold  $tol$ , the learning rate  $\tau_t$  at each step, and a small constant  $\hat{\epsilon}$ .
- 2: Initialize  $t=0$  and  $\mathcal{M}_0^{(\tilde{k})} = \mathcal{V}_0^{(\tilde{k})} = (0, \dots, 0)^T \in \mathbb{R}^{2m}$ .
- 3: Compute the displacement field  $u[\ell_{h'}^0]$  by employing the direct-line method, and subsequently evaluate the regularized energy functional  $J_\nu^0$  using expression (3.7).
- 4: **do**
- 5:   for  $\tilde{k}=1, \dots, \tilde{K}$
- 6:     Compute  $\mathcal{G}_t^{(\tilde{k})}$  via (3.8).
- 7:      $\mathcal{M}_{t+1}^{(\tilde{k})} = (1 - \hat{\beta}_1) \mathcal{G}_t^{(\tilde{k})} + \hat{\beta}_1 \mathcal{M}_t^{(\tilde{k})}$ .
- 8:      $\mathcal{V}_{t+1}^{(\tilde{k})} = (1 - \hat{\beta}_2) \mathcal{G}_t^{(\tilde{k})} \odot \mathcal{G}_t^{(\tilde{k})} + \hat{\beta}_2 \mathcal{V}_t^{(\tilde{k})}$ , where  $\mathcal{G}_t^{(\tilde{k})} \odot \mathcal{G}_t^{(\tilde{k})}$  returns the element wise square.
- 9:      $\tilde{\mathcal{M}}_{t+1}^{(\tilde{k})} = \mathcal{M}_{t+1}^{(\tilde{k})} / (1 - (\hat{\beta}_1)^{t+1})$ .
- 10:      $\tilde{\mathcal{V}}_{t+1}^{(\tilde{k})} = \mathcal{V}_{t+1}^{(\tilde{k})} / (1 - (\hat{\beta}_2)^{t+1})$ .
- 11:      $\mathcal{L}_{t+1}^{(\tilde{k})} = \mathcal{L}_t^{(\tilde{k})} - \tau_t \tilde{\mathcal{M}}_{t+1}^{(\tilde{k})} / (\sqrt{\tilde{\mathcal{V}}_{t+1}^{(\tilde{k})}} + \hat{\epsilon})$ .
- 12:     Set  $t := t + 1$ .
- 13:     Compute the displacement field  $u[\ell_{h'}^t]$  by employing the direct-line method, and subsequently evaluate the regularized energy functional  $J_\nu^t$  using expression (3.7).
- 14: **while**  $\frac{|J_\nu^t - J_\nu^{t-1}|}{|J_\nu^{t-1}|} > tol$ .
- 15: **Output:**  $\mathcal{L}_{\tilde{n}}^{(\tilde{k})}$ ,  $\tilde{n} > 0$  is a certain positive integer.

---

The regularized minimization problem (3.5) presents several computational challenges that guide our choice of optimizer. First, the energy functional  $J_\nu(\ell_h')$  is defined over a high-dimensional parameter space  $\Lambda_{h'}$ , with the number of parameters scaling with the angular discretization  $m'$ . Second, the total variation regularization term, while essential for promoting piecewise-constant solutions, introduces a non-smoothness that must be handled. Although the smoothing parameter  $\nu$  mitigates this, the objective function can still exhibit complex, non-convex landscapes and varying curvature across different parameters. To address these challenges, we employ the Adam optimization algorithm [36]. Adam is particularly well-suited for this problem.

## 4 Numerical examples

### 4.1 Numerical experiments for forward problems

Numerical solutions and eigenvalues are computed by semi-discretization of linear elements, while reference values are obtained by discretization of quadratic elements on refined meshes in Examples 4.1-4.3. We define the  $L^2$  norm  $\|\cdot\|_2$  and energy norm  $\|\cdot\|_*$  by

$$\|v\|_2 = \left( \iint_{\Omega} (|v_1|^2 + |v_2|^2) dx dy \right)^{1/2}, \quad \|v\|_* = \left( \iint_{\Omega} (2\mu|\varepsilon(v)|^2 + \lambda|\nabla \cdot v|^2) dx dy \right)^{1/2},$$

We can conclude that for any  $v \in H^1(\Omega) \times H^1(\Omega)$ , the inequality  $\|v\|_* \leq \|v\|_*$  holds, where  $\|\cdot\|_*$  has been defined in Theorem 2.1. We will judge the feasibility of our model by the energy relative error  $\frac{\|u-u^h\|_*}{\|u\|_*}$  and  $L^2$  relative error  $\frac{\|u-u^h\|_2}{\|u\|_2}$ , where  $u^h = (u_1^h, u_2^h)^T$  is the numerical solution measured using the direct-line method and  $u = (u_1, u_2)^T$  is approximated as the reference/exact solution.

#### Example 4.1.

Let the boundary functions be defined as:

$$\tilde{r}^{(1)}(\phi) = \begin{cases} \frac{1}{\sqrt{\sin^4(\phi) + \cos^4(\phi)}}, & \pi/4 < \phi \leq 7\pi/4, \\ -\frac{1}{\sin(\phi - \frac{\pi}{2})}, & -\pi/4 < \phi \leq \pi/4, \end{cases}$$

$$\tilde{r}^{(2)}(\phi) = \begin{cases} \frac{1}{\sqrt{\sin^4(\phi) + \cos^4(\phi)}}, & -3\pi/4 < \phi \leq 3\pi/4, \\ -\frac{1}{\sin(\phi + \frac{\pi}{2})}, & 3\pi/4 < \phi \leq 5\pi/4, \end{cases}$$

with  $\Omega^{(\tilde{k})} = \{(r, \phi) | 0 \leq r < \tilde{r}^{(\tilde{k})}(\phi), 0 \leq \phi < 2\pi, \tilde{k}=1,2\}$ ,  $\Omega_i^{(\tilde{k})} = \{(r, \phi) | 0 < r < \tilde{r}^{(\tilde{k})}(\phi), \theta_i^{(\tilde{k})} < \phi < \theta_{i+1}^{(\tilde{k})}, i=1,2\}$ ,  $\theta_1^{(1)} = -\pi, \theta_2^{(1)} = -\pi/4, \theta_3^{(1)} = \pi$ , and  $\theta_1^{(2)} = 0, \theta_2^{(2)} = 3\pi/4, \theta_3^{(2)} = 2\pi$ .

The lamé coefficients here are  $(\mu_1^{(1)}, \lambda_1^{(1)}) = (0.1, 1)$ ,  $(\mu_2^{(1)}, \lambda_2^{(1)}) = (0.6, 2)$ ,  $(\mu_1^{(2)}, \lambda_1^{(2)}) = (0.1, 1)$ ,  $(\mu_2^{(2)}, \lambda_2^{(2)}) = (0.6, 2)$ ; And the body force  $p = (1, 1)^T$  and the Dirichlet boundary condition  $f = (y^2, -x^2)^T$ . see Figure 4.

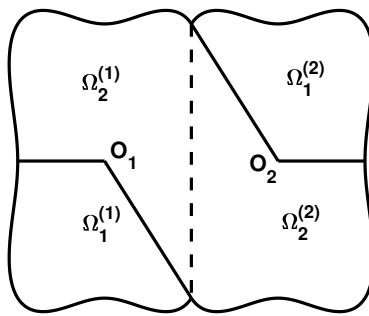
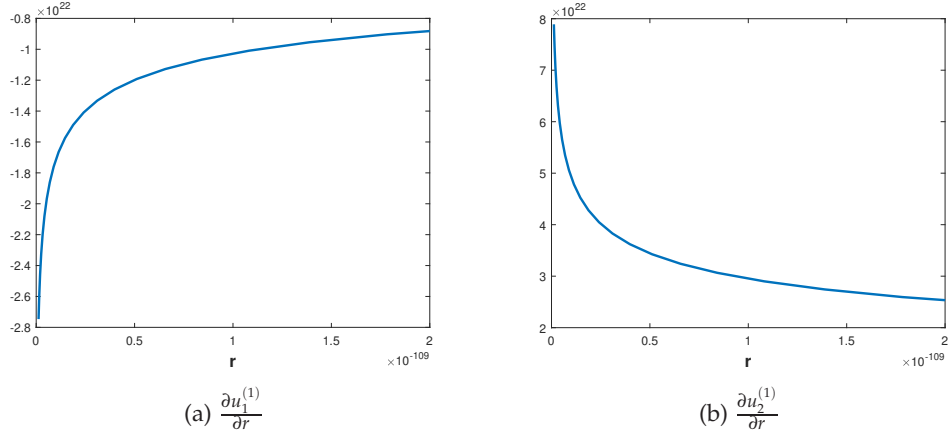


figure 4: Domain  $\Omega$  in Example 4.1

We show  $\frac{\partial u}{\partial r}(r, \phi_0)$  with  $\phi_0 = \frac{3\pi}{4}$  in Figure 5. It can be observed that as  $r \rightarrow 0$ , the derivatives  $\frac{\partial u_1^{(1)}}{\partial r}$  and  $\frac{\partial u_2^{(1)}}{\partial r}$  tend to  $-\infty$  and  $\infty$ , respectively. This behavior confirms the presence of stress singularities at the singular point.

figure 5:  $\frac{\partial u}{\partial r}(r, \phi_0)$  with  $\phi_0 = \frac{3\pi}{4}$  in Example 4.1

The errors of the first non-zero eigenvalue  $\gamma_3^h$  relative to the reference value  $\gamma_3 = 0.7775070808$  are provided in Table 1. As the mesh refines, exhibiting a second-order convergence rate. This result indicates that the eigenvalues can achieve quadratic convergence towards exact eigenvalues, proving the method's natural ability to capture singularities. The  $L^2$  and energy relative errors are shown in Table 2. The  $L^2$  error converges at a rate of 2, while the energy error converges linearly. These results align with Theorem 2.1, which guarantees first-order convergence in the energy norm and second-order in the  $L^2$  norm for linear elements, even in the presence of stress singularities.

table 1: Errors of  $\gamma_3^h$ , with  $\gamma_3 = 0.7775070808$ 

M	$ \gamma_3^h - \gamma_3 $	order
16	1.638e-2	–
32	3.835e-3	2.094
64	9.181e-4	2.063
128	2.268e-4	2.018
256	5.654e-5	2.005

table 2: Convergence order of relative error between  $L^2$  and energy

M	$\frac{\ u - u^h\ _2}{\ u\ _2}$	order	$\frac{\ u - u^h\ _*}{\ u\ _*}$	order
16	7.229e-2	–	8.208e-2	–
32	2.304e-2	1.649	3.324e-2	1.304
64	6.277e-3	1.877	1.497e-2	1.151
128	1.660e-3	1.919	7.094e-3	1.078
256	4.552e-4	1.867	3.415e-3	1.055

### Example 4.2.

Let the boundary functions be defined as:

$$\tilde{r}^{(1)}(\phi) = \begin{cases} \frac{1}{\sqrt{\sin^4(\phi) + \cos^4(\phi)}}, & -\pi/4 < \phi \leq 3\pi/4, \\ -\frac{1}{\sin(\phi + \frac{\pi}{2})}, & 3\pi/4 < \phi \leq 5\pi/4, \\ -\frac{1}{\sin(\phi)}, & -3\pi/4 < \phi \leq -\pi/4, \end{cases}$$

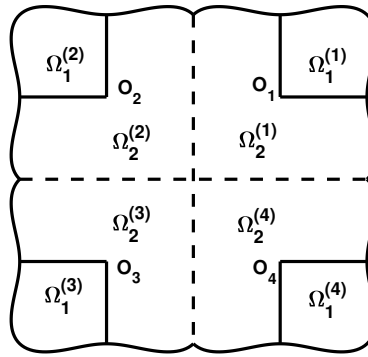
$$\tilde{r}^{(2)}(\phi) = \begin{cases} \frac{1}{\sqrt{\sin^4(\phi) + \cos^4(\phi)}}, & \pi/4 < \phi \leq 5\pi/4, \\ -\frac{1}{\sin(\phi)}, & -3\pi/4 < \phi \leq -\pi/4, \\ -\frac{1}{\sin(\phi - \frac{\pi}{2})}, & -\pi/4 < \phi \leq \pi/4, \end{cases}$$

$$\tilde{r}^{(3)}(\phi) = \begin{cases} \frac{1}{\sqrt{\sin^4(\phi) + \cos^4(\phi)}}, & 3\pi/4 < \phi \leq 7\pi/4, \\ -\frac{1}{\sin(\phi - \frac{\pi}{2})}, & -\pi/4 < \phi \leq \pi/4, \\ -\frac{1}{\sin(\phi - \pi)}, & \pi/4 < \phi \leq 3\pi/4, \end{cases}$$

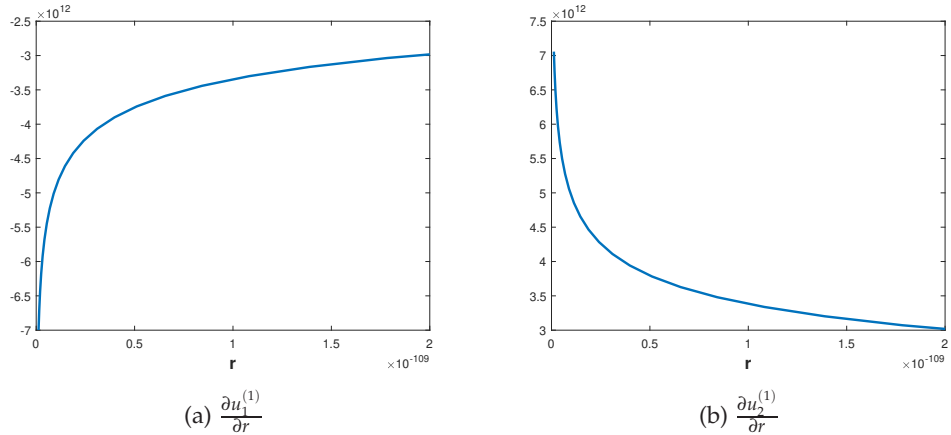
$$\tilde{r}^{(4)}(\phi) = \begin{cases} \frac{1}{\sqrt{\sin^4(\phi) + \cos^4(\phi)}}, & -3\pi/4 < \phi \leq \pi/4, \\ -\frac{1}{\sin(\phi - \pi)}, & \pi/4 < \phi \leq 3\pi/4, \\ -\frac{1}{\sin(\phi + \frac{\pi}{2})}, & 3\pi/4 < \phi \leq 5\pi/4, \end{cases}$$

with  $\Omega_i^{(\tilde{k})} = \{(r, \phi) | 0 < r < \tilde{r}^{(\tilde{k})}(\phi), \theta_i^{(\tilde{k})} < \phi < \theta_{i+1}^{(\tilde{k})}, \tilde{k} = 1, \dots, 4, i = 1, 2\}$ ,  $\theta_1^{(1)} = 0, \theta_2^{(1)} = \pi/2, \theta_3^{(1)} = 2\pi; \theta_1^{(2)} = -\pi, \theta_2^{(2)} = \pi/2, \theta_3^{(2)} = \pi; \theta_1^{(3)} = -\pi, \theta_2^{(3)} = -\pi/2, \theta_3^{(3)} = \pi$ ; and  $\theta_1^{(4)} = 0, \theta_2^{(4)} = 3\pi/2, \theta_3^{(4)} = 2\pi$ .

The lamé coefficients here are  $(\mu_1^{(1)}, \lambda_1^{(1)}) = (0.6, 2)$ ,  $(\mu_2^{(1)}, \lambda_2^{(1)}) = (0.1, 1)$ ;  $(\mu_1^{(2)}, \lambda_1^{(2)}) = (0.7, 2.1)$ ,  $(\mu_2^{(2)}, \lambda_2^{(2)}) = (0.1, 1)$ ;  $(\mu_1^{(3)}, \lambda_1^{(3)}) = (0.6, 2)$ ,  $(\mu_2^{(3)}, \lambda_2^{(3)}) = (0.1, 1)$ ;  $(\mu_1^{(4)}, \lambda_1^{(4)}) = (0.5, 1.9)$ ,  $(\mu_2^{(4)}, \lambda_2^{(4)}) = (0.1, 1)$ ; And the body force  $p = (1, 1)^T$  and the Dirichlet boundary condition  $f = (1, 1)^T$ . see Figure 6.

figure 6: Domain  $\Omega$  in Example 4.2

We show  $\frac{\partial u}{\partial r}(r, \phi_0)$  with  $\phi_0 = \frac{\pi}{4}$  in Figure 7. It can be observed that as  $r \rightarrow 0$ , the derivatives  $\frac{\partial u_1^{(1)}}{\partial r}$  and  $\frac{\partial u_2^{(1)}}{\partial r}$  tend to  $-\infty$  and  $\infty$ , respectively. This behavior confirms the presence of stress singularities at the singular point.

figure 7:  $\frac{\partial u}{\partial r}(r, \phi_0)$  with  $\phi_0 = \frac{\pi}{4}$  in Example 4.2

The errors of the first non-zero eigenvalue  $\gamma_3^h$  relative to the reference value  $\gamma_3 = 0.8333347413$  are provided in Table 3. As the mesh refines, exhibiting a second-order convergence rate. This result indicates that the eigenvalues can achieve quadratic convergence towards exact eigenvalues, proving the method's natural ability to capture singularities. The  $L^2$  and energy relative errors are shown in Table 4. The  $L^2$  error converges at a rate of 2, while the energy error converges linearly. These results align with Theorem 2.1, which guarantees first-order convergence in the energy norm and second-order in the  $L^2$  norm for linear elements, even in the presence of stress singularities.

table 3: Errors of  $\gamma_3^h$ , with  $\gamma_3 = 0.8333347413$ 

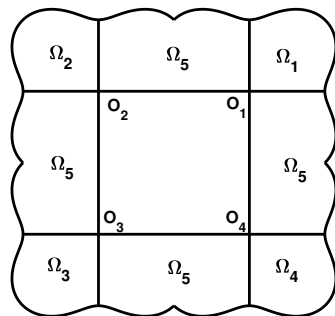
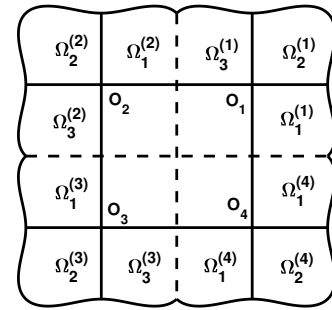
M	$ \gamma_3^h - \gamma_3 $	order
16	5.594e-2	–
32	3.173e-2	0.818
64	1.035e-2	1.616
128	2.811e-3	1.881
256	7.186e-4	1.968

table 4: Convergence order of relative error between  $L^2$  and energy

M	$\frac{\ u - u^h\ _2}{\ u\ _2}$	order	$\frac{\ u - u^h\ _*}{\ u\ _*}$	order
16	3.441e-2	–	3.795e-2	–
32	1.215e-2	1.502	1.538e-2	1.303
64	3.267e-3	1.896	5.991e-3	1.361
128	8.397e-4	1.961	2.678e-3	1.163
256	2.139e-4	1.973	1.293e-3	1.051

### Example 4.3.

Here, the middle is empty,  $\Omega = \bigcup \Omega_k, k=1, \dots, 5$ ,  $\Omega = \bigcup \Omega^{(\tilde{k})}, \tilde{k}=1, \dots, 4$ , and  $\Omega^{(\tilde{k})} = \bigcup \Omega_i^{(\tilde{k})}, i=1, 2, 3$ . see Figure 8.

(a) Domain  $\Omega$ (b) Subdomain  $\Omega^{(\tilde{k})}$ figure 8: Decomposition of domain  $\Omega$  into subdomains with a central void and four singular points.

Let the boundary functions be defined as:

$$\tilde{r}^{(1)}(\phi) = \begin{cases} -\frac{1}{\sin(\phi)}, & -\pi/2 \leq \phi \leq -\pi/4, \\ \sqrt{1+\sin^2(2\phi)}, & -\pi/4 < \phi \leq 3\pi/4, \\ -\frac{1}{\sin(\phi+\frac{\pi}{2})}, & 3\pi/4 < \phi \leq \pi, \end{cases}$$

$$\tilde{r}^{(2)}(\phi) = \begin{cases} -\frac{1}{\sin(\phi-\frac{\pi}{2})}, & 0 \leq \phi \leq \pi/4, \\ \sqrt{1+\sin^2(2\phi)}, & \pi/4 < \phi \leq 5\pi/4, \\ -\frac{1}{\sin(\phi)}, & -3\pi/4 < \phi \leq -\pi/2, \end{cases}$$

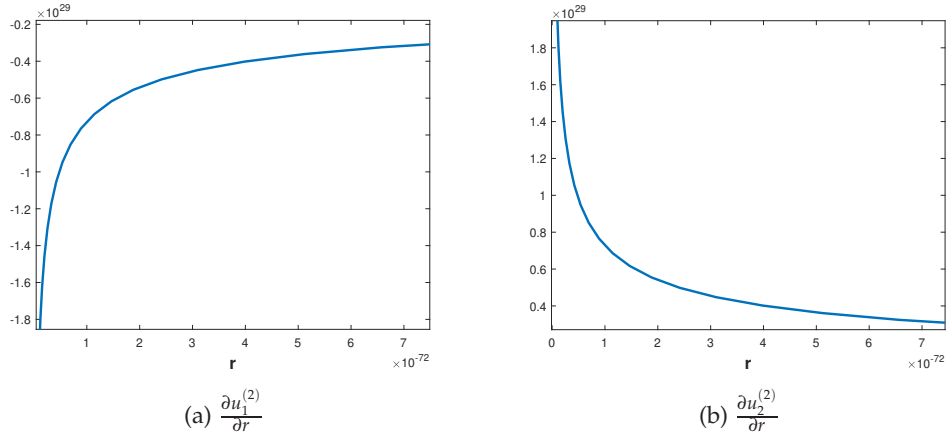
$$\tilde{r}^{(3)}(\phi) = \begin{cases} -\frac{1}{\sin(\phi-\pi)}, & \pi/2 \leq \phi \leq 3\pi/4, \\ \sqrt{1+\sin^2(2\phi)}, & 3\pi/4 < \phi \leq 7\pi/4, \\ -\frac{1}{\sin(\phi-\frac{\pi}{2})}, & -\pi/4 < \phi \leq 0, \end{cases}$$

$$\tilde{r}^{(4)}(\phi) = \begin{cases} -\frac{1}{\sin(\phi+\frac{\pi}{2})}, & -\pi \leq \phi \leq -3\pi/4, \\ \sqrt{1+\sin^2(2\phi)}, & -3\pi/4 < \phi \leq \pi/4, \\ -\frac{1}{\sin(\phi-\pi)}, & \pi/4 < \phi \leq \pi/2, \end{cases}$$

with  $\Omega_i^{(\tilde{k})} = \{(r, \phi) | 0 < r < \tilde{r}^{(\tilde{k})}(\phi), \theta_i^{(\tilde{k})} < \phi < \theta_{i+1}^{(\tilde{k})}, \tilde{k} = 1, \dots, 4, i = 1, 2, 3\}$ ,  $\theta_1^{(1)} = -\pi/2, \theta_2^{(1)} = 0, \theta_3^{(1)} = \pi/2, \theta_4^{(1)} = \pi; \theta_1^{(2)} = 0, \theta_2^{(2)} = \pi/2, \theta_3^{(2)} = \pi, \theta_4^{(2)} = 3\pi/2; \theta_1^{(3)} = \pi/2, \theta_2^{(3)} = \pi, \theta_3^{(3)} = 3\pi/2, \theta_4^{(3)} = 2\pi; \text{ and } \theta_1^{(4)} = -\pi, \theta_2^{(4)} = -\pi/2, \theta_3^{(4)} = 0, \theta_4^{(4)} = \pi/2$ .

The lamé coefficients here are  $(\mu_1^{(1)}, \lambda_1^{(1)}) = (0.4, 1), (\mu_2^{(1)}, \lambda_2^{(1)}) = (0.6, 1.5), (\mu_3^{(1)}, \lambda_3^{(1)}) = (0.4, 1); (\mu_1^{(2)}, \lambda_1^{(2)}) = (0.4, 1), (\mu_2^{(2)}, \lambda_2^{(2)}) = (0.6, 1.5), (\mu_3^{(2)}, \lambda_3^{(2)}) = (0.4, 1); (\mu_1^{(3)}, \lambda_1^{(3)}) = (0.4, 1), (\mu_2^{(3)}, \lambda_2^{(3)}) = (0.6, 1.5), (\mu_3^{(3)}, \lambda_3^{(3)}) = (0.4, 1); (\mu_1^{(4)}, \lambda_1^{(4)}) = (0.4, 1), (\mu_2^{(4)}, \lambda_2^{(4)}) = (0.6, 1.5), (\mu_3^{(4)}, \lambda_3^{(4)}) = (0.4, 1)$ ; And the body force  $p = (\frac{x}{\sqrt{x^2+y^2}}, \frac{y}{\sqrt{x^2+y^2}})^T$  and the Dirichlet boundary condition  $f = (1, 1)^T$ .

We show  $\frac{\partial u}{\partial r}(r, \phi_0)$  with  $\phi_0 = \frac{3\pi}{4}$  in Figure 9. It can be observed that as  $r \rightarrow 0$ , the derivatives  $\frac{\partial u_1^{(2)}}{\partial r}$  and  $\frac{\partial u_2^{(2)}}{\partial r}$  tend to  $-\infty$  and  $\infty$ , respectively. This behavior confirms the presence of stress singularities at the singular point.

figure 9:  $\frac{\partial u}{\partial r}(r, \phi_0)$  with  $\phi_0 = \frac{3\pi}{4}$  in Example 4.1

The errors of the first non-zero eigenvalue  $\gamma_3^h$  relative to the reference value  $\gamma_3 = 0.5713189037$  are provided in Table 5. As the mesh refines, exhibiting a second-order convergence rate. This result indicates that the eigenvalues can achieve quadratic convergence towards exact eigenvalues, proving the method's natural ability to capture singularities. The  $L^2$  and energy relative errors are shown in Table 6. The  $L^2$  error converges at a rate of 2, while the energy error converges linearly. These results align with Theorem 2.1, which guarantees first-order convergence in the energy norm and second-order in the  $L^2$  norm for linear elements, even in the presence of stress singularities.

table 5: Errors of  $\gamma_3^h$ , with  $\gamma_3 = 0.5713189037$ 

M	$ \gamma_3^h - \gamma_3 $	order
16	4.846e-3	
32	1.308e-3	1.890
64	3.305e-4	1.985
128	8.287e-5	1.997
256	2.073e-5	1.999

table 6: Convergence order of relative error between  $L^2$  and energy

M	$\frac{\ u - u^h\ _2}{\ u\ _2}$	order	$\frac{\ u - u^h\ _*}{\ u\ _*}$	order
16	1.339e-3	–	3.501e-3	–
32	5.161e-4	1.375	1.899e-3	0.882
64	1.409e-4	1.873	9.838e-4	0.949
128	3.598e-5	1.969	4.972e-4	0.984
256	8.835e-6	2.026	2.491e-4	0.997

Numerical experiments (examples 4.1-4.3) show that the eigenvalues using direct-line method converge rapidly to the true eigenvalue of elliptic operator, confirming its inherent ability of this

method to solve for singularities. Notably, even under the condition that there are multiple stress singularities in general regions, optimal convergence rates are achieved for linear/quadratic elements. These results collectively validate the effectiveness and precision of the proposed approach for modeling linear elasticity in composite materials within general domains.

## 4.2 Numerical experiments for inverse elasticity problems

Next, our numerical experiment use the Adam Algorithm 3.1 to minimize (3.7) over  $\ell_{h'} \in \Lambda_{h'}$ , with some parameter settings as follows:  $tol = 5 \times 10^{-6}$ ,  $\hat{\beta}_1 = 0.9$ ,  $\hat{\beta}_2 = 0.999$ ,  $\eta = 10^{-7}$ ,  $\nu = 10^{-7}$ ,  $\hat{\epsilon} = 10^{-7}$  and a decaying  $\tau_k$ . And set the grid size  $h' = \pi/64$  to discretize the solution space, that is

$$\mu_{h'} = \mathbb{1}_{(-\infty, 0]}(\rho) \sum_{j=1}^{128} \mu_j \mathbb{1}_{[(j-1)h', jh']}( \phi ), \quad \lambda_{h'} = \mathbb{1}_{(-\infty, 0]}(\rho) \sum_{j=1}^{128} \lambda_j \mathbb{1}_{[(j-1)h', jh']}( \phi ).$$

Here, we use  $\mu_j^k$  and  $\lambda_j^k$  to represent the values of  $\mu_j$  and  $\lambda_j$  in step  $k$  respectively. At each iteration, each iteration is solving a forward problem (mesh parameter  $h' = \pi/64$ ). For validation purposes, reference solutions  $u[\ell^*]$  are computed using quadratic elements on refined meshes via the same direct-line method, providing noise-free benchmark results. The measurement data are collected at discrete points within the domain  $\Omega$ , denoted by the set  $\Xi = \{(x_j, y_j)\}_{j=1}^{M_1} \subset \Omega$ . To quantify the precision of the reconstructed Lamé coefficients, the  $L^1$  error is used, where the  $L^1$  norm is represented by  $\|\cdot\|_1$ .

### Example 4.4.

Building on the analysis of the forward problem in Example 4.1, we now investigate the corresponding inverse elasticity problem to estimate the Lamé coefficients from displacement measurements.

The noisy measurement is defined as  $z|_{\Xi} = \delta \xi_U \|u[\ell^*]\|_{\infty} + u[\ell^*]|_{\Xi}$ , where  $\|\cdot\|_{\infty}$  denotes in  $L^{\infty}$  norm,  $\delta = 0.0001$  represents the noise level and  $\xi_U$  is a vector of independent identically distributed uniform random variables on  $[-1, 1]$ . The initial values are set as  $\mu_1^0 = \dots = \mu_{128}^0 = 0.35$ ,  $\lambda_1^0 = \dots = \lambda_{128}^0 = 1.5$ . The iteration process continues for 842 steps until the termination criterion is met. Figure 10 reflects the change in the value of  $J$ , which converges gradually with the iteration step number  $k$ . The numerically reconstructed Lamé coefficients  $\mu_{h'}^{842}$  and  $\lambda_{h'}^{842}$  along the  $\phi$ -direction is represented by the blue broken line in Figure 11, and the true values are indicated by the red dotted lines. In the 842nd iteration, the error results are  $\|\mu_{h'}^{842} - \mu^*\|_1 / \|\mu^*\|_1 = 7.873e-3$  and  $\|\lambda_{h'}^{842} - \lambda^*\|_1 / \|\lambda^*\|_1 = 1.111e-2$ .

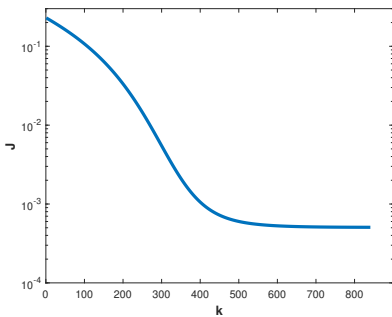


figure 10: Convergence of the objective function  $J$  in Example 4.4

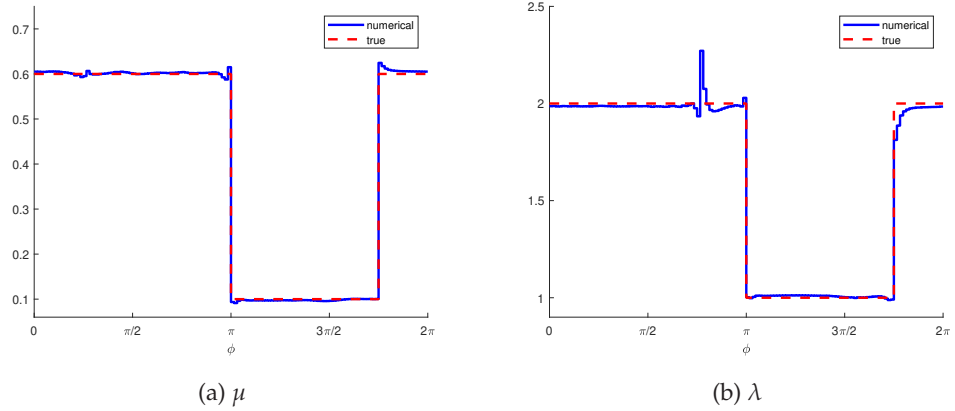
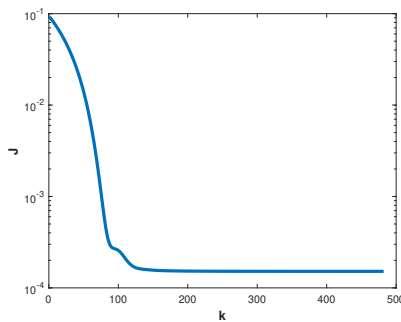


figure 11: Reconstructed Lamé coefficients and true Lamé coefficients

#### Example 4.5.

Building upon the forward problem analysis in Example 4.2, we now investigate the corresponding inverse elasticity problem to estimate the Lamé coefficients from displacement measurements.

The noisy measurement is defined as  $z|_{\Xi} = \delta \xi_U \|u[\ell^*]\|_{\infty} + u[\ell^*]|_{\Xi}$ , where  $\|\cdot\|_{\infty}$  denotes in  $L^{\infty}$  norm,  $\delta = 0.0001$  represents the noise level and  $\xi_U$  is a vector of independent identically distributed uniform random variables on  $[-1, 1]$ . The initial values are set as  $\mu_1^0 = \dots = \mu_{128}^0 = 0.35, \lambda_1^0 = \dots = \lambda_{128}^0 = 1.5$ . The iteration process continues for 482 steps until the termination criterion is met. Figure 12 reflects the change in the value of  $J$ , which converges gradually with the iteration step number  $k$ . The numerically reconstructed Lamé coefficients  $\mu_{h'}^{482}$  and  $\lambda_{h'}^{482}$  along the  $\phi$ -direction is represented by the blue broken line in Figure 13, and the true values are indicated by the red dotted lines. At the 482nd iteration, the error results are:  $\|\mu_{h'}^{482} - \mu^*\|_1 / \|\mu^*\|_1 = 8.223\text{e-}3$  and  $\|\lambda_{h'}^{482} - \lambda^*\|_1 / \|\lambda^*\|_1 = 4.132\text{e-}3$ .

figure 12: Convergence of the objective function  $J$  in Example 4.5

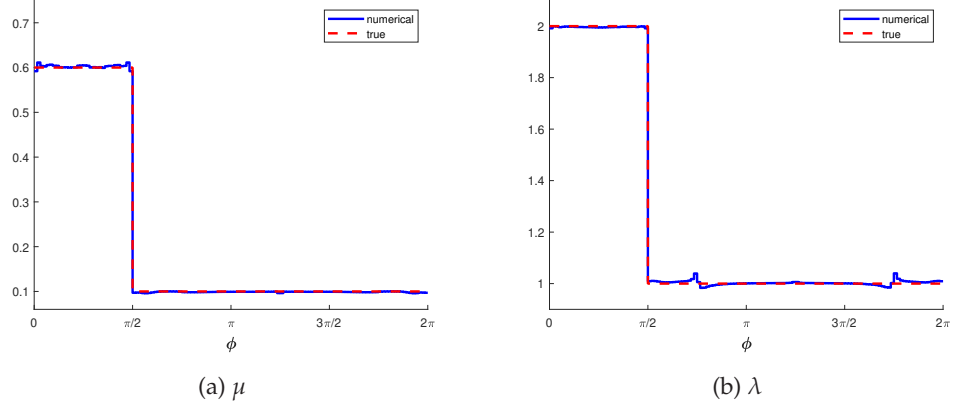
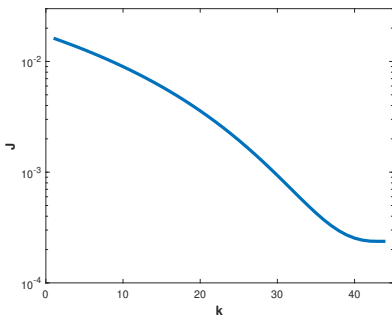


figure 13: Reconstructed Lamé coefficients and true Lamé coefficients

#### Example 4.6.

Building upon the forward problem analysis in Example 4.3, we now investigate the corresponding inverse elasticity problem to estimate the Lamé coefficients from displacement measurements. The noisy measurement is defined as  $z|_{\Xi} = \delta \xi_U \|u[\ell^*]\|_{\infty} + u[\ell^*]|_{\Xi}$ , where  $\|\cdot\|_{\infty}$  denotes in  $L^{\infty}$  norm,  $\delta = 0.0001$  represents the noise level and  $\xi_U$  is a vector of independent identically distributed uniform random variables on  $[-1,1]$ . The initial values are set as  $\mu_1^0 = \dots = \mu_{128}^0 = 0.35, \lambda_1^0 = \dots = \lambda_{128}^0 = 1.25$ . The iteration process continues for 44 steps until the termination criterion is met. Figure 14 reflects the change in the value of  $J$ , which converges gradually with the iteration step number  $k$ . The numerically reconstructed Lamé coefficients  $\mu_h^{44}$  and  $\lambda_h^{44}$  along the  $\phi$ -direction is represented by the blue broken line in Figure 15, and the true values are indicated by the red dotted lines. At the 44nd iteration, the error results are:  $\|\mu_h^{44} - \mu^*\|_1 / \|\mu^*\|_1 = 5.087\text{e-}3$  and  $\|\lambda_h^{44} - \lambda^*\|_1 / \|\lambda^*\|_1 = 7.737\text{e-}3$ .

figure 14: Convergence of the objective function  $J$  in Example 4.6

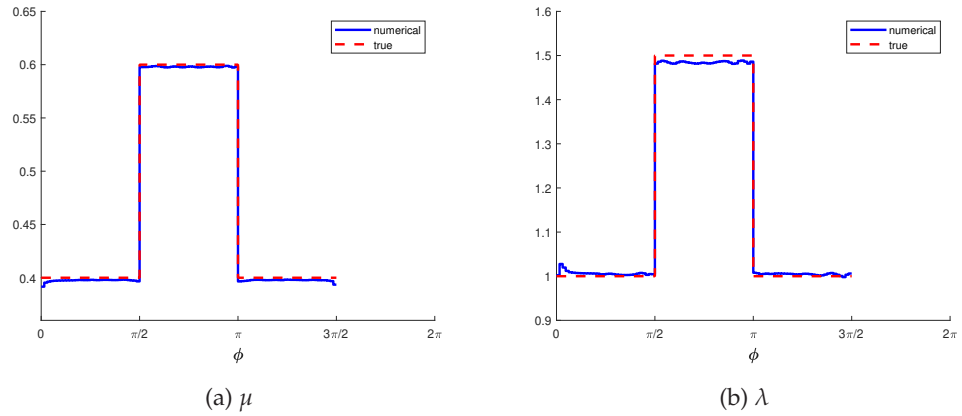


figure 15: Reconstructed Lamé coefficients and true Lamé coefficients

#### Example 4.7.

According to Example 4.6, we will focus on the impact of measurement noise on the effectiveness and accuracy of the proposed Algorithm. We choose  $\delta = 0.0003, 0.0007, 0.001, 0.01$ .

table 7: Error results under different noises

$\delta$	$\tilde{k}$	$\ \mu_{h'}^{\tilde{k}} - \mu^*\ _1 / \ \mu^*\ _1$	$\ \lambda_{h'}^{\tilde{k}} - \lambda^*\ _1 / \ \lambda^*\ _1$
0.0003	44	5.095e-3	7.310e-3
0.0007	44	5.108e-3	7.355e-3
0.001	44	5.509e-3	7.311e-3
0.01	45	8.091e-3	1.702e-2

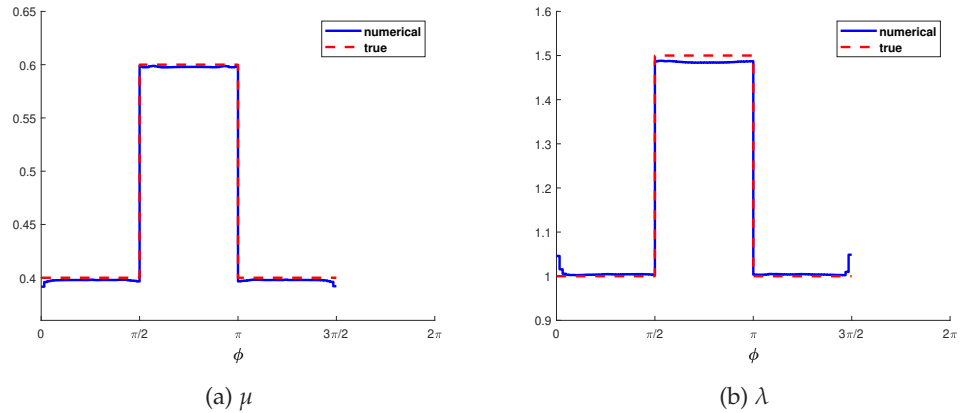


figure 16: Reconstructed Lamé coefficients and true Lamé coefficients

For the case with noise level  $\delta = 0.0001$ , the reconstructed Lamé coefficients (see Figure 15) show excellent agreement with the true values. The corresponding results for higher noise levels ( $\delta = 0.0003, \delta = 0.0007, \delta = 0.001$  and  $\delta = 0.01$ ) exhibited comparable accuracy in interface identification, though with slightly increased oscillations in the reconstructed parameter profiles near the

material boundaries. (see Figure 16, here, only the image of  $\delta = 0.0003$  is shown). Table 7 presents the convergence behavior under different noise levels  $\delta$ . In particular, our method is feasible and applicable to slight noise levels and different types of noise.

## 5 Conclusion

This work proposes a novel computational framework that extends the direct-line method and domain decomposition techniques to linear elastic problems with multiple singular points in general domains and applies it to inverse elastic problems. Domain decomposition technology views the general domain as the union of two or more star-shaped subdomains. Assuming that the boundaries of each subdomain can be described by explicit  $C^1$  parameter curves in polar coordinates, we transform the irregular star-shaped subdomain into a regular semi-infinite strip through coordinate transformation, thereby transforming our problem into a variational differential problem. And after discretizing the angular variable to obtain a semi-discrete approximation, we use the direct-line methods for analytical solution. Numerical results demonstrate that the eigenvalues converge rapidly to those of the exact elliptic operator, thus naturally capturing singularities, and this method possesses optimal error estimation capabilities. Numerical results confirm the accuracy and computational efficiency of the proposed method for general domains containing multiple singular points.

For inverse problems, this work addresses the inverse elasticity problem of composite materials by estimating piecewise constant Lamé coefficients through the minimization of an energy functional combined with total variation regularization. The optimization is implemented using the Adam algorithm. At every optimization step, the forward simulation is formulated as a linear elastic problem with multiple singular points on general domain. To handle geometric irregularities and potential multiple singularities, the direct-line method is employed as the forward solver. Numerical experiments demonstrate that the proposed approach accurately reconstructs both interface locations and Lamé coefficients distributions across all subdomains.

## Acknowledgments

This work was partially supported by the NSFC Project No. 12025104, Liaoning Provincial Natural Science Foundation Project No. 2025-BS-0410 and Liaoning Provincial Department of Education Project No. LJ212410147018.

## References

- [1] I. Babuška, R.B. Kellogg and J. Pitkäranta, Direct and inverse error estimates for finite elements with mesh refinements *Numer. Math.*, 33 (1979), 447-471.
- [2] P.P.L. Matos, R.M. Mcmeeking, P.G. Charalambides and M.D. Drory, A method for calculating stress intensities in bimaterial fracture, *Int. J. Fract.*, 40 (1989), 235-254.
- [3] H. Han et al, The numerical solutions of interface problems by infinite element method, *Numer. Math.*, 39 (1989), 39-50.

- [4] Z. Li and R. Mathon, Error and stability analysis of boundary methods for elliptic problems with interfaces, *Math. Comp.*, 54 (1990), 41-61.
- [5] S.T. Raveendra and P.K. Banerjee , Computation of stress intensity factors for interfacial cracks, *Eng. Fract. Mech.*, 40 (1991), 89-103.
- [6] G.J. Fix, S. Gulati and G.I. Wakoff , On the use of singular functions with finite element approximations, *J. Comput. Phys.*, 13(1973), 209-228.
- [7] K.Y. Lin and J.W. Mar , Finite element analysis of stress intensity factors for cracks at a bi-material interface, *Int. J. Fract.* 12 (1976), 521-531.
- [8] H.-S. Oh and I. Babuška, The method of auxiliary mapping for the finite element solutions of elasticity problems containing singularities, *J. Comput. Phys.*, 121 (1995), 193-212.
- [9] C. Carstensen, G. Dolzmann, S.A. Funken and D. Helm, Locking-free adaptive mixed finite element methods in linear elasticity, *Comput. Methods Appl. Mech. Engrg.*, 190 (2000), 1701-1718.
- [10] T.P. Wihler et al, Locking-free adaptive discontinuous Galerkin FEM for linear elasticity problems, *Math. Comp.*, 75 (2006), 1087-1102.
- [11] Zhao J, Hou Y, Song L, Modified intrinsic extended finite element method for elliptic equation with interfaces, *Journal of Engineering Mathematics*, 97 (2016), 147-159.
- [12] Y.K. Cheung and C.P. Jiang, Application of the finite strip method to plane fracture problems, *Eng. Fract. Mech.*, 53 (1996), 89-96.
- [13] V. Gupta, C.A. Duarte, I. Babuška and U. Banerjee, A stable and optimally convergent generalized FEM (SGFEM) for linear elastic fracture mechanics, *Comput. Methods Appl. Mech. Engrg.*, 266 (2013), 23-39.
- [14] S.S. Ghorashi, N. Valizadeh and S. Mohammadi, Extended isogeometric analysis for simulation of stationary and propagating cracks, *Int. J. Numer. Methods Eng.*, 89 (2012) 1069-1101.
- [15] Guidault, P-A. et al, A multiscale extended finite element method for crack propagation, *Computer Methods in Applied Mechanics and Engineering*, 197 (2008), 381-399.
- [16] W.E. Schiesser, The numerical method of lines: integration of partial differential equations, Elsevier, (2012).
- [17] L.S. Xanthis, C. Schwab, The method of arbitrary lines, *C.R. Acad. Sci., Série 1, Mathématique*, 312 (1991), 181-187.
- [18] Kozlov, Vladimir, Elliptic boundary value problems in domains with point singularities, American Mathematical Soc, Vol 52 (1997).
- [19] Z. Wu, Z. Huang, W.-C. Wang, Y. Yang, The direct method of lines for elliptic problems in star-shaped domains, *J. Comput. Appl. Math.*, 327 (2018), 350-361.
- [20] Zhu, Xiaopeng, Zhizhang Wu, and Zhongyi Huang, The direct method of lines for forward and inverse linear elasticity problems of composite materials in star-shaped domains, *Numer. Math. Theory Methods Appl.*, 16 (2013), 242-276.
- [21] Han, Houde, and Zhongyi Huang, The discrete method of separation of variables for composite material problems, *International journal of fracture*, 112.4 (2001), 379-402.
- [22] Mohseni, Kamran, and Tim Colonius, Numerical treatment of polar coordinate singularities, *Journal of Computational Physics*, 157 (2000), 787-795.
- [23] Keyes, David E., and William D. Gropp, A comparison of domain decomposition techniques for elliptic partial differential equations and their parallel implementation, *SIAM Journal on Scientific and Statistical Computing*, 8 (1987), s166-s202.
- [24] Lloberas-Valls, et al, Domain decomposition techniques for the efficient modeling of brittle heterogeneous materials, *Computer Methods in Applied Mechanics and Engineering*, 200 (2011), 1577-1590.
- [25] Dryja, Maksymilian, and Olof B. Widlund, Some domain decomposition algorithms for elliptic problems, *Iterative methods for large linear systems*, (1990), 273-291.
- [26] van den Boom, Sanne J., et al. "A stable interface-enriched formulation for immersed domains with

strong enforcement of essential boundary conditions." *International Journal for Numerical Methods in Engineering* 120.10 (2019): 1163-1183.

- [27] Aminpour, Mohammad A., Jonathan B. Ransom, and Susan L. McCleary. "A coupled analysis method for structures with independently modelled finite element subdomains." *International Journal for Numerical Methods in Engineering* 38.21 (1995): 3695-3718.
- [28] Bonnet, Marc, and Andrei Constantinescu. "Inverse problems in elasticity." *Inverse problems* 21.2 (2005): R1.
- [29] Grediac, Michel. "The use of full-field measurement methods in composite material characterization: interest and limitations." *Composites Part A: applied science and manufacturing* 35.7-8 (2004): 751-761.
- [30] Grédiac, Michel, and François Hild, eds. *Full-field measurements and identification in solid mechanics*. John Wiley and Sons, 2012.
- [31] Parker, Kevin J., Marvin M. Doyley, and Deborah J. Rubens. "Imaging the elastic properties of tissue: the 20 year perspective." *Physics in medicine biology* 56.1 (2010): R1.
- [32] Ju, Shen-Haw, C. Y. Chiu, and C. C. Lu, Determination of stress intensity factors for multi-material junctions, *International journal of fracture*, 171 (2011), 23-34.
- [33] Eberle, Sarah, et al, 2021 Lipschitz stability estimate and reconstruction of Lamé parameters in linear elasticity, *Inverse Problems in Science and Engineering*, 29.3 (2021), 396-417.
- [34] M. Gockenbach and A. Khan, An abstract framework for elliptic inverse problems: Part 1. An output least-squares approach, *Math. Mech. Solids*, 12 (2007), 259-276.
- [35] Vogel, Curtis R. *Computational methods for inverse problems*. Society for Industrial and Applied Mathematics, 2002.
- [36] Kingma, Diederik P. "Adam: A method for stochastic optimization." *arXiv preprint arXiv:1412.6980* (2014).
- [37] Jadamba, Baasansuren, Akhtar A. Khan, and Fabio Raciti. "On the inverse problem of identifying Lamé coefficients in linear elasticity." *Computers Mathematics with Applications* 56.2 (2008): 431-443.